Thermal Performance Of Termite Mold Bricks Reinforced With Empty Fruit Bunch Spikelet And Coconut Fibers

Wannyuy Kingsly Mofor[1,4*], Yakum Reneta Nafu[1,2.], Tchemou Gilbert[2.], Ngonge Viyof Wilfred[1], Foba Josepha Tendo[3]

[1]Department Of Mechanical Engineering, Higher Technical Teacher Training College, The University Of Bamenda Bambili, Cameroon
[2]Laboratory Of Mechanics And Adapted Materials (Lamma), University Of Douala, Douala, Cameroon
[3]Department Of Chemistry, Faculty Of Science, University Of Buea, Buea, Cameroon
[4]Laboratory Of Mechanics, Doctorate School Of Fundamental And Applied Sciences, University Of Douala, Douala, Cameroon
*Corresponding Author: Wannyuy kingsly mofor
kingslymofor@yahoo.com

Abstract
The use of natural fibers to enhance the thermal properties of earth bricks has become increasingly popular. This study investigates the thermal performance of termite mold soil (TMS) reinforced with two types of fibers: coconut fibers (CF) and empty fruit bunch spikelet fibers (EFBSF). Various fiber compositions (0%, 0.5%, 1%, 1.5%, 2%, and 2.5%) were combined with sodium hydroxide (NaOH) treatments at concentrations of 1%, 2%, 3%, and 4%. Laboratory results reveal that TMS exhibits promising physical properties, including a moisture content of 23.64%, a maximum dry density of 1.63 g/cm³, and a plasticity index of 20%, indicating its structural stability and suitability for earth block production. The study also analyzes the chemical properties of EFBSF and CF fibers, noting that CF has a higher holocellulose content (88.0%) compared to EFBSF (33.5%), which impacts moisture retention and structural integrity. Thermal analysis demonstrates that incorporating these natural fibers significantly enhances the thermal performance of TMS. With a 2.5% fiber content, CF reduces thermal effusivity from 1771.43 J/m²Ks^1/2 to 1079.39 J/m²Ks^1/2 and thermal conductivity from 0.86 W/mK to 0.38 W/mK, making it particularly effective in improving insulation in hot conditions. EFBSF also lowers thermal effusivity and conductivity, but to a lesser extent than CF. Additionally, the presence of these fibers reduces volumetric calorific capacity, with CF showing a more pronounced effect. Overall, TMS reinforced with coconut fibers, especially at 1% NaOH and 2.5% fiber content, offers the best thermal performance, suggesting its potential for sustainable construction. This research promotes the use of locally sourced, natural fibers in earth block manufacturing, contributing to the development of more energy-efficient and environmentally friendly building materials.
Keywords: Thermal Characterization, Termite Mould Soil, Natural Fibers Reinforcement, Earth Block Production

I. Introduction

The demand for sustainable building materials has increased in recent years, driven by rising environmental concerns and the requirement for energy-efficient construction methods. Conventional construction materials like burnt bricks and concrete have notable environmental consequences, including substantial energy consumption and the release of greenhouse gases throughout their manufacturing process. [6,7] As a result, both researchers and industry are actively investigating alternative materials that can provide similar performance while also minimizing their impact on the environment. Out of these options, bio-based composites have emerged as attractive contenders for sustainable building. [8, -11] The use of agricultural wastes in the manufacturing of construction materials has attracted interest because of its plentiful supply, capacity to be renewed, and potential to address waste disposal problems. Agricultural leftovers, such as empty fruit bunch spikelet (EFBS) and coconut fibers, are very desirable because of their abundant presence in locations where palm oil and coconut production are widespread. These waste products, known as residues, can be converted into valuable resources by undergoing suitable processing and being integrated into construction

materials.[14] An example of an inventive use is utilizing agricultural waste to create bricks made from termite mold. Termite mold bricks, or termite mound bricks, are bricks that are shaped and designed to imitate the structure and characteristics of termite mounds.[13] Termite mounds are well-known for their thermal characteristics, which offer natural insulation and temperature control.[30] The researchers want to improve the thermal performance of termite mold bricks by integrating agricultural wastes, while also making use of the plentiful agricultural waste.

The thermal characteristics of construction materials have a crucial role in the energy efficiency of buildings, affecting both the amount of heat needed for heating and the amount of cooling required. Improved thermal insulation minimizes the requirement for artificial heating and cooling, resulting in reduced energy consumption and operational expenses. [16] Furthermore, enhanced thermal characteristics play a significant role in ensuring a comfortable indoor environment and promoting the well-being of occupants, hence making it an essential factor to consider in sustainable building design. Prior research has investigated different agricultural residues in building materials, emphasizing their capacity to improve mechanical durability, thermal insulation, and moisture control.[17,2] Research on coconut fiber-reinforced composites has shown enhancements in mechanical qualities, including increased flexural and compressive strength, as well as improved heat conductivity when used in building materials.[27-28]Studies on the byproducts of the palm oil industry have demonstrated encouraging findings about their ability to provide thermal insulation and resistance to fire when included into composite materials. [31-32] This research article examines the thermal efficiency of termite mold bricks that are strengthened by agricultural residue, with a specific emphasis on empty fruit bunch spikelet and coconut fibers. The study seeks to evaluate the impact of various agricultural wastes on the thermal conductivity, heat storage capacity, and overall thermal efficiency of the termite mold bricks. The project seeks to add to the expanding knowledge on sustainable building materials and provide insights into the practicality of utilizing agricultural leftovers to improve thermal performance by analyzing these features. the thermal performance of termite mold bricks that are strengthened with agricultural residues. The use of agricultural leftovers shows potential for sustainable construction approaches, providing advantages in terms of reducing environmental impact, improving resource efficiency, and enhancing building performance.[33] This study seeks to enhance our comprehension and utilization of bio-based composites in the construction industry through empirical research and analysis.

By doing so, it hopes to contribute to sustainable development objectives and the progression of environmentally friendly building technologies.

II. Materials And Methods

Materials
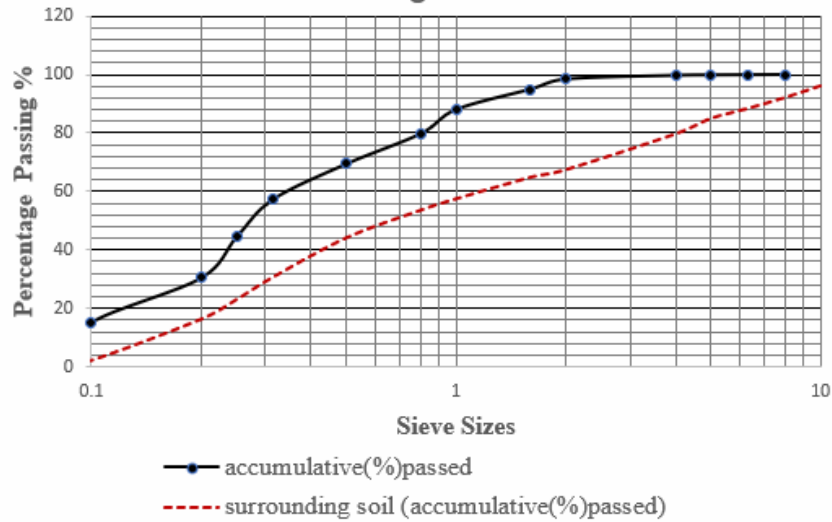
Soil

termite mound soil (TMS) was gathered from termite mounds situated near New Road Bamenda in the Northwest region of Cameroon (6°1'38N, 10°1'2E). and Physio Mechanical Characterization was carried at the GEOSTRUCT Laboratory Nkwen Bamenda according to NFP 94-050.Fig 1 illustrates the TMS characterization: A) Specific gravity (B) Determination of Atterberg's limit (C) Grain size analysis
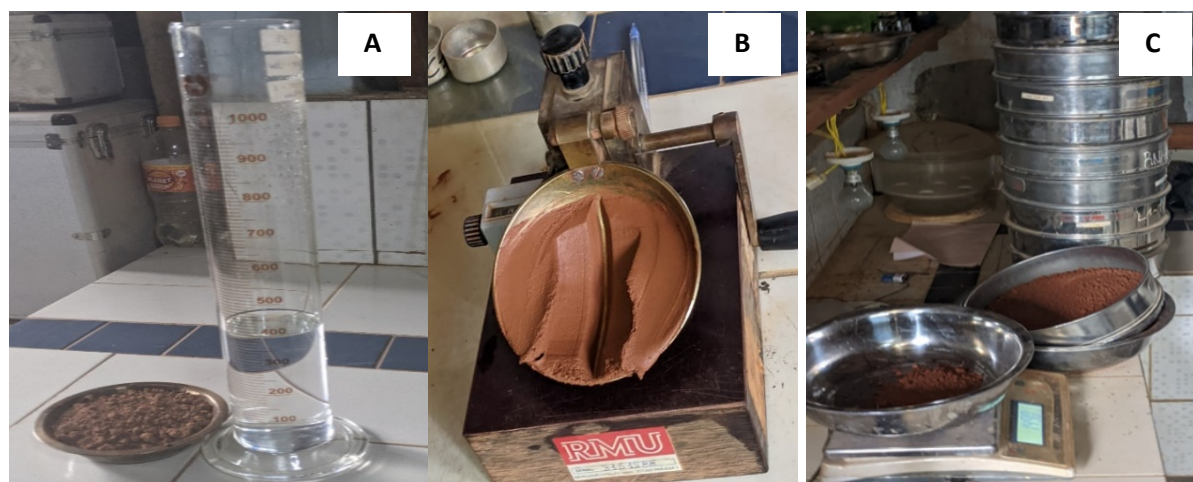
Figure 1: TMS characterization (A) Specific gravity (B) Determination of Atterberg's limit (C) Grain size analysis

Figure 2 displays the particle size distribution curve for TMS and the surrounding soils. The comparative investigation of soil particle distribution is depicted in this picture, which sheds lights on the textural variations between TMS and surrounding soils.

Figure 2. Distribution curve of particle size of TMS and surrounding soils

Fibres

The empty fruit bunch spikelet fibres (EFBSF) and coconut fibres (CF) used in this study were sourced from a palm oil mill in Bamunka, located in Ndop subdivision of the Northwest region Cameroon. EFBSF and CF were treated with sodium hydroxide of concentration (1%, 2%, 3%, and 4%) at the University of Buea Chemistry Laboratory. The EFBSF were immersed in the solution and continuously stirred for 10 minutes before being thoroughly washed with water and dried under sunlight for 5 hours, followed by additional drying in an oven at 105 degrees Celsius for 24 hours. After drying, the fibers were carefully removed and stored on polythene papers for later composite formation. This process is depicted in figure 3 below [20-21].
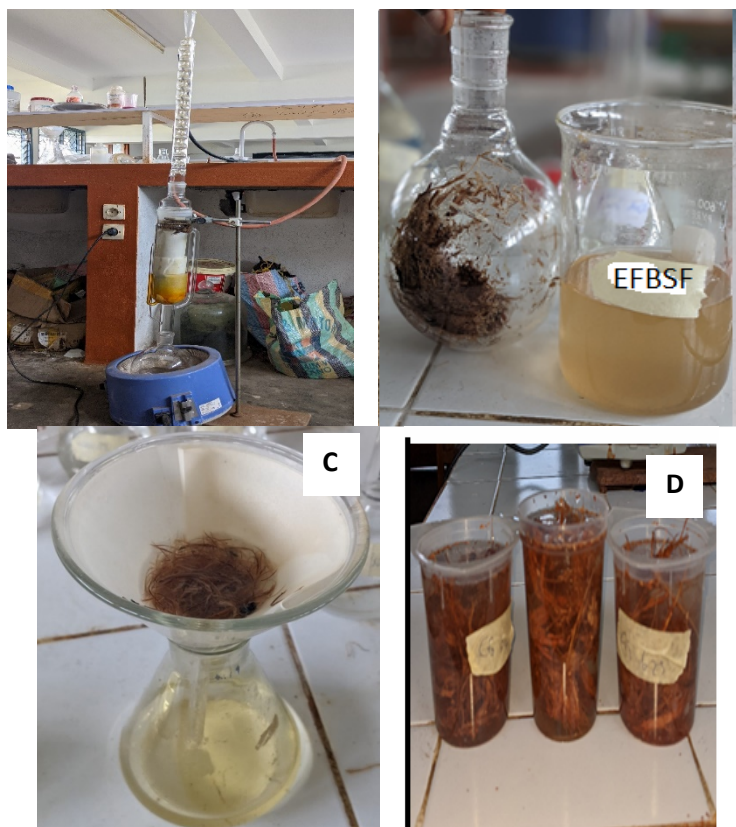

Figure 3: Extracted EFBSF and CF(A) Pretreating fibres (B) Oven drying of treated fibres(C)

The Soxhlet method for dewaxing, pectin testing, hemicellulose and cellulose determination, and water absorption measurement are all shown Figure 4 below.

A   **B**

Figure 4: Soxhlet Process de waxing (A), Pectin Testing (B), Hemicellulose and cellulose determination(C), Water Absorption determination (D)

Sample preparation

Fiber content of 0%, 0.5%,1%,1.5% 2% and 2.5% was incorporated into termite mound soil (TMS) using oil palm EFB spikelet and coconut fibers to reinforce the bricks. Initially, the soil underwent manual grinding and sieving through a 1.6mm mesh sieve. Meanwhile, EFB spikelet and coconut fibers were manually trimmed to a uniform length of 5cm using scissors, following the methodology described by [26] The dry soil sample was subsequently sifted and transferred into a basin, where fiber percentages were carefully measured and recorded before being mixed with 52g of water. The resulting mixture was then placed in to fabricated molds sized at 100x100x20mm and compacted. Each formulation involved creating 10 samples, varying fiber percentages from 0% to 2.5%, (E1- E5) and sodium hydroxide treatments from 1% to 4% for both types of fibers (A1 to A4 for EFBSF) (B1 to B4 for CF). The changes in the mass composition of empty fruit bunch (EFBSF) and coconut fibres (CF) samples utilized in the investigation are presented in Table 1 below

Table 1 displays the changes in the mass composition of the EFBSF and CF samples utilized in the investigation.

NOAH pretreatment	designation of sample	Mass of Soil(g)	Water (%)	Mass of Fibers(g)	Fibre ratio (%)	Length Of fibres(cm)
A1- A4 B1-B4	E0	325	52	0	0	5
	E1	323.4	52	1.625	0.5	5
	E2	321.8	52	3.25	1	5
	E3	320.1	52	4.875	1.5	5
	E4	318.5	52	6.5	2	5
	E5	316.9	52	8.125	2.5	5

Samples used for thermal testing procedures or thermal analysis are illustrated on figure 5 below

A   **B**
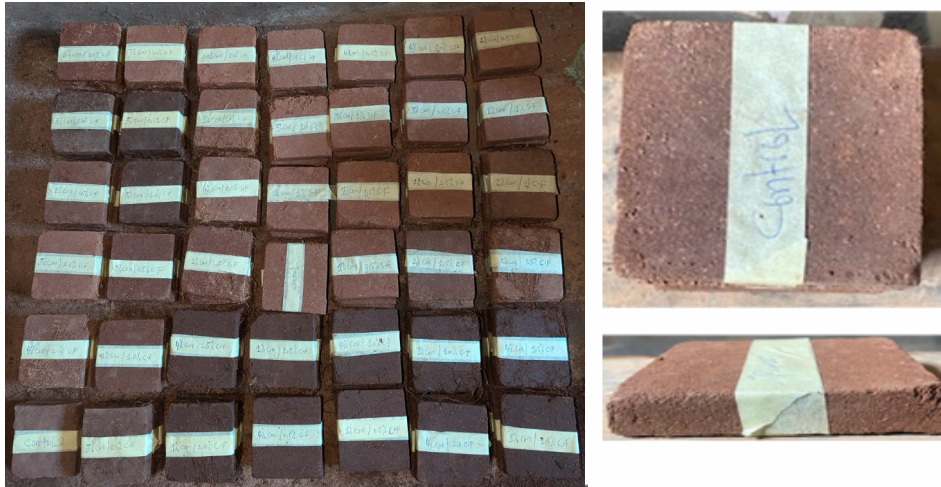
Figure 5: Samples for thermal testing

Estimation of thermophysical parameters using the asymmetric hot plate method.

The work intends to assess thermal effusivity, volumetric heat capacity (ρC_p), and estimate thermal conductivity of the material using experimental methods. The asymmetric hot plate approach was used for thermal characterization, which involved: Conducting experiments to determine how the material's temperature varies in response to rapid variations in heat flux. The analysis of two experimental thermographs aids in calculating the thermal conductivity. Creating a model of the experimental setup and applying techniques like de Hoog and Levenberg-Marquart to estimate the material's thermal conductivity. When experimental and modelled results demonstrate a strong correlation, the findings' accuracy is validated. [1,23,28-29]

Thermal Parameters Estimated

a) Thermal Effusivity

Thermal effusivity (E), defined by equation (1) with unit's J/m^2K^2s^1/2, represents the combined influence of thermal conduction on temperature change and the effect of energy storage (Cp). Increased thermal conductivity improves the transfer of heat from the surroundings, while higher heat capacity at a steady pressure restricts the rise in internal temperature, facilitating the storage of heat. This parameter quantifies the rate at which the surface temperature of a material increases. Higher values indicate that the material absorbs heat quickly while experiencing minimal increase in internal temperature.

$$E = \sqrt{\lambda \, \rho \, C_p}$$

(1)

b) Specific heat capacity,

Specific heat capacity, or specific heat, quantifies a substance's capability to absorb thermal energy and undergo a corresponding rise in temperature. Understanding how materials react to different temperatures is of utmost importance. The quantification of specific heat capacity is expressed in joules per kilogramme kelvin and is represented by equation (2). Within some thermal situations, the term "volumetric heat capacity" is used to describe the ability of a material to store heat within a specific volume. This measurement is expressed in joules per cubic metre per kelvin (J/m3 K).

$$C_p = \frac{1}{m} \frac{dQ}{dt}$$

(2)

Thermal conductivity (λ), measured in W/mK, quantifies how well heat moves through a material in steady conditions. It reflects the material's resistance to heat flow: lower values indicate better thermal insulation properties. The thermal conductivity was determined by equation 3

$$\lambda = \frac{E^2}{\rho C_p} \quad ou \quad \lambda_{est} = \frac{\left(E^2\right)_{est}}{\left(\rho C_p\right)_{est}}$$

(3)

Where est:value estimated by characterization

d) Thermal diffusivity (α)

Thermal diffusivity (α) is a measurement, expressed in m²/s that assesses the speed at which a temperature wave propagates through a material by conduction. A lower value of α indicates a lesser thermal

conductivity of the material, resulting in a longer time for heat to propagate from one side to the other. This feature is crucial for comprehending heat transfer phenomena. It is utilized to enhance understanding of the properties of materials for particular applications and temperature computations when accuracy is crucial. It was determined by equation 4
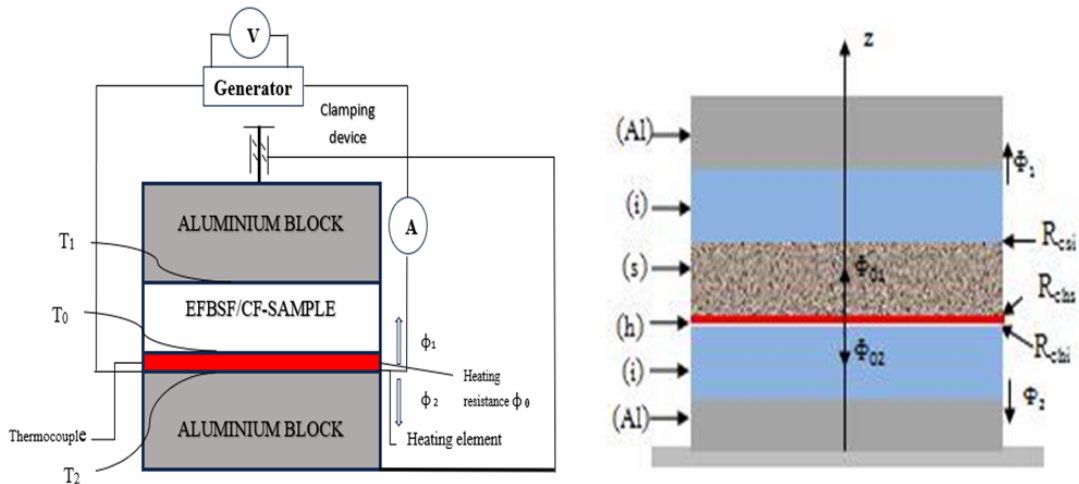
$$a = \frac{\lambda}{\rho C_p}$$

(4)

Experimental Measurement Device

The experimental setup of the asymmetric hot plate used in the study is as shown in figure 6 and figure 7below

1- Hoist (frame), 2-Clamping device, 3-Sample, 4-Heating resistor, 5-Insulators, 6- Stabilized power supply, 7- Temperature recorder.

Figure 6: Experimental Setup: Asymmetric Hot Plat

Figure 7: (a) **Experimental model device (b) Asymmetric Hot Plate Experimental Device (Cross-Sectional View) [3]**

The experimental setup employs a "MINCO 230Ω P" heating resistor positioned between two flat material samples. Both the heating probe and sample ideally share the same surface area to ensure unidirectional heat transfer with minimal lateral convective losses. A type K thermocouple measures the temperature at the interface. A voltage generator applies a thermal flux step, and a Picolog probe records the

temperature evolution at the probe's center. This setup assumes unidirectional heat transfer at the sample's center until lateral disturbances occur. [8,18-19]

1D Quadripolar Modeling for a Semi-Infinite (SI) Model: Temperature at the Center of the Probe for the Semi-Infinite Model
We consider the asymmetric hot plate model represented in figure 8
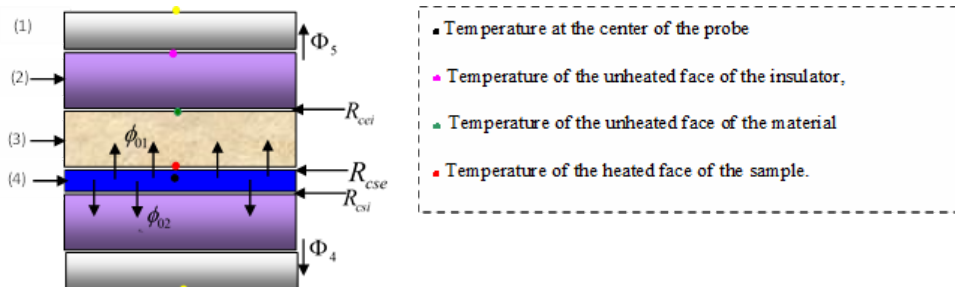

Figure 8: Hot plate experimental setup (1) Aluminum block; (2) Insulating material; (3) Sample to be characterized; (4) Heating resistor; Rc is the contact resistance [18]

The experimental setup involving a hot plate where the lateral dimensions of the resistor are significantly larger than the sample thickness. This allows for one-directional heat transfer at the probe center, modeled using the quadrupole method. Initially, convective losses 'h' at the sample's lateral faces are disregarded. The setup treats the probe as a thin system, ensuring uniform temperature across its thickness. Key components include an aluminum block, insulating material, the sample for testing, and a heating resistor. Contact resistances Rc_1, Rc_2, and Rc_3 are specified for interfaces between the probe and sample, sample and insulator, and probe and insulator, respectively as shown in equation 5 [22-25]

$$\begin{pmatrix} \theta_0 \\ \Phi_{01} \end{pmatrix} = [M_1][M_2][M_3] \tag{5}$$

$\theta_0 = L(T_0(x,t))$: is the Laplace transform of the temperature rise at the probe level

$\Phi_{01} = L(\phi_0(x,p))$: is the Laplace transform of the heat flux density dissipated upwards in the sample.

M_1 : is the element representing half the thickness of the prob as expressed by equation 6

$$[M_1] = \begin{pmatrix} 1 & 0 \\ \dfrac{m_s c_s}{S} p & 1 \end{pmatrix} = \begin{pmatrix} 1 & 0 \\ \rho_s c_s e_s p & 1 \end{pmatrix} \tag{6}$$

M_2 : is the element representing the contact resistance at the probe-sample interface. Determined by equation 7

$$[M_2] = \begin{pmatrix} 1 & SR_{cse} \\ 0 & 1 \end{pmatrix} \tag{7}$$

M_3 : is the element representing the material considered as semi-infinite based on equation 8

$$[M_3] = \begin{pmatrix} \theta_3 \\ E\sqrt{p}\theta_3 \end{pmatrix} \tag{8}$$

The quadrupole method applied to the downward flux is formulated, taking into account the insulator as a semi-infinite material as well. Shown in equation 9

$$\begin{pmatrix} \theta_0 \\ \Phi_{02} \end{pmatrix} = [M_4][M_5] \tag{9}$$

Φ_{02} : is the Laplace transform of the heat flux density dissipated downwards in the sample.

M_4 : is the element representing the contact resistance at the probe-insulator interface as expressed in equation 10

$$[M_4] = \begin{pmatrix} 1 & SR_{csi} \\ 0 & 1 \end{pmatrix}$$

(10)

M_5 : is the element representing the insulating material considered as semi-infinite using equation 11

$$[M_5] = \begin{pmatrix} \theta_4 \\ E_i \sqrt{p} \theta_4 \end{pmatrix}$$

(11)

The total flux density equation 12 is given by the relationship:

$$\phi_0 = \phi_1 + \phi_2$$

(12)

By combining all these different matrices, we arrive at the relationship that represents the theoretical response of the semi-infinite asymmetric hot plate model in the Laplace domain determined by equation 13

$$\theta_{SI}(x, p) = \frac{\phi_0 S}{p} \cdot \frac{1}{\frac{\rho_s c_s e_s Sp + (1 + R_{chs} \rho_s c_s e_s Sp) ES\sqrt{p}}{1 + R_{chs} ES\sqrt{p}} + \frac{E_i S\sqrt{p}}{1 + R_{chi} E_i S\sqrt{p}}}$$

(13)

$\theta_{SI}(x, p)$ is the Laplace transform of the temperature at the center of the probe $T_{model\,SI}(x, t) = L^{-1}(\theta_{SI}(x, p))$

A simplified estimation at long times ($p \to 0$, simplified model), From equation (13), a simplified model allows obtaining in the real space the evolution of the temperature at the center of the material. it is determined by equation 14

$$\Delta T(0, t \to \infty) = \phi_0 S \left(\frac{E^2 R_{chs} + E_i^2 R_{chi}}{(E + E_i)^2} - \frac{\rho_s c_s e_s}{S(E + E_i)^2} \right) + \frac{2\phi_0}{(E + E_i) \cdot \sqrt{\pi}} \sqrt{t}$$

(14)

The numerical calculation of the slope $\alpha(t) = \frac{\Delta T(t + dt) - \Delta T(t)}{\sqrt{t + dt} - \sqrt{t}}$ of the curve T=f(t^{1/2}), thus allows obtaining a preliminary estimate (pre-est) of the thermal effusivity of the material given by the relation (15).

$$E_{preest} = \frac{2\phi_0}{\alpha \sqrt{\pi}} - E_i$$

(15)

We can also preliminarily estimate the volumetric heat capacity ρC_p from the simplified model using equation 16. The heat transfer δq through the probe during a time interval dt infinitely small corresponds to a heat flux $\rho_0 = {\delta q}/{dt}$, which causes a temperature rise dT in the probe. By utilizing the linear part of the thermogram T=f(t), we can numerically calculate its slope β and thus deduce the pre-estimated value of the volumetric heat capacity of the sample using the relationship of equation 16:

$$\left(\rho C_p \right)_{preest} = \frac{\frac{\phi_o}{\beta} - \rho C_{pi} e_i - \rho C_{ps} e_s}{e}$$

(16)

The pre-estimations of E and ρCp will allow us to determine the apparent thermal conductivity of the materials using the relationship (17).

$$\lambda_{preest} = \frac{\left(E^2 \right)_{preest}}{\left(\rho C_p \right)_{preest}}$$

(17)

Asymmetric 1D quadripolar models for the complete model.

Temperature at the center of the probe for the complete model. $T_{model}(x, t)$
We still consider the scheme from Figure 8. Applying the formalism of quadripoles, we have

---

$$\begin{pmatrix} \theta_0 \\ \Phi_{01} \end{pmatrix} = [M_1][M_2][M_6][M_7][M_8] \begin{pmatrix} \theta_5 \\ \Phi_5 \end{pmatrix} = \begin{pmatrix} A & B \\ C & D \end{pmatrix} \begin{pmatrix} \theta_5 \\ \Phi_5 \end{pmatrix} \qquad (18)$$

M_6 : is the element representing the material to be characterized as represented by equation 19

$$[M_6] = \begin{pmatrix} A_e & B_e \\ C_e & D_e \end{pmatrix} \qquad (19)$$

$$A_e = \cosh(q_e \cdot e) \quad B_e = \frac{\sinh(q_e \cdot e)}{\lambda_e \cdot q_e} \qquad q = \sqrt{\frac{p \rho C_p}{\lambda}}$$

With: $C_e = \lambda_e \cdot q_e \cdot \sinh(q_e \cdot e) \quad D_e = A_e$ $\qquad (20)$

M_7 : is the element representing the contact at the interface between the sample and the insulation. Equation 21

$$[M_7] = \begin{pmatrix} 1 & SR_{cei} \\ 0 & 1 \end{pmatrix} \qquad (21)$$

M_8 : is the element representing the insulation material

$$[M_8] = \begin{pmatrix} A_i & B_i \\ C_i & D_i \end{pmatrix} \qquad (22)$$

With :

$$A_i = \cosh(q_i \cdot e_i) \quad B_i = \frac{\sinh(q_i \cdot e_i)}{\lambda_e \cdot q_i}$$

$$C_i = \lambda_i \cdot q_i \cdot \sinh(q_i \cdot e_i) \quad D_i = A_i \qquad (23)$$

The role of the aluminum block here is to maintain the temperature constant at the interface between the insulation material and the aluminum block. Now, if we evaluate the Biot number of this block using

$$(Bi)_{bloc} = \frac{h_{bloc} \cdot b}{\lambda_{bloc}}$$

relation (24) $\qquad (24)$

With the values h_{bloc}=10 W/m²K, k=200k = 200k=200 W/mK, b=100 mm, we find b=0.005, which is well below 0.1. In this case, we can consider it as uniform. Therefore:

$$\theta_5(x,p) = L(\Delta T(x,p))_{bloc} = 0$$

$$\theta_4(x,p) = L(\Delta T(x,p))_{bloc} = 0 \qquad (25)$$

Similarly, in equation (2), we replace the matrix element M with the matrix M thus equation 26:

$$\begin{pmatrix} \theta_0 \\ \Phi_{02} \end{pmatrix} = [M_4][M_8] \begin{pmatrix} \theta_4 \\ \Phi_4 \end{pmatrix} \qquad (26)$$

By combining equations (5), (15), and (22), we found the temperature at the center of the probe in Laplace space, given by equation (23):

$$\theta_0(x,p) = \frac{\phi_0}{p} \cdot \frac{1}{\dfrac{D}{B} + \dfrac{D_i}{B_i + R_{csi}D_i}} \qquad (27)$$

The Levenberg-Marquardt algorithm (1944), integrated into a Matlab code, allows us to estimate the value of E that minimizes the sum of squared errors of the functional ψ.

$$\psi = \sum_{i=1}^{n} \left[\Delta T_{\exp}(t_i) - T_{\text{model}}(t_i) \right]^2 \qquad (28)$$

between the experimental curve $\Delta T_{exp}(t) = T(0,t) - T_a$ and the theoretical curve

$T_{\text{model}}(x,t) = L^{-1}(\theta_0(x,p))$

Determination of the thermal capacity **Cp**

Knowing the experimental volumetric mass density ρ_{exp} and the estimated volumetric heat capacity ρC_p, we can estimate the heat capacity C_p using the relationship and calculated using equation 29

$$C_p = \frac{(\rho C_p)_{mod\,elcomplet}}{\rho_{exp}}$$

(29)

III. Results And Discussions

Physio-Mechanical Characterization of Soil

The physio-mechanical characterization of the collected soil revealed a moisture content of 23.64% and a maximum dry density of 1.63 g/cm³. The Atterberg limits were determined to be a liquid limit of 46% and a plastic limit of 26%, resulting in a plasticity index of 20%. The soil exhibited an organic content of 15.66%, a neutral pH value of 7, and a specific gravity of 2.50. The optimum moisture content for compaction was found to be 22%. Sedimentation analysis indicated a ratio of 5.2:3.2:1.4, and the soil passed the cigarette test with a result of 6.92. Furthermore, sieve analysis demonstrated that the majority of particles were distributed within the clay soil region.

Chemical Characterization of EFBSF and CF

The chemical characterization of EFBSF and CF revealed significant details: EFBSF exhibited 33.5% holocellulose, 24.6% hemicellulose, 40.6% cellulose, and 11.59% lignin, with a moisture content of 13.7% and a water absorption rate of 64.73%. CF, on the other hand, contained 88% holocellulose, 37.2% hemicellulose, 50.8% cellulose, and 9.25% lignin, with a moisture content of 14.56% and a water absorption rate of 81.53%.

Thermal Characteristics of EFBSF AND CF reinforced bricks
The determination of thermal conductivity is carried out in several steps.

Experimental thermogram of temperatures

We utilized a temperature step P = UI by means of the generator (Figure 6), leading to a rise in temperature at the centre of the probe." The temperature thermograms in Figure 9 were acquired experimentally by applying heat to the heating resistor in the control sample (C). The Picolog probe, outfitted with a thermocouple, documented the progression of temperature at the core of the material. The thermogram Texp was analyzed using linear regression in Excel, which enabled the estimation of λexp using equations (15) and (16).
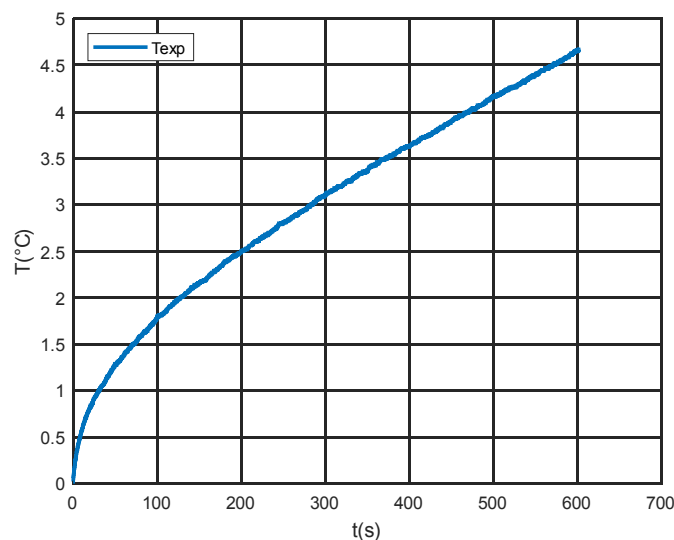

Figure 9 : Experimental temperature thermogram for the control sample

Pre-estimation of E and ρCp: Temperature thermogram obtained with the simplified model

When examining the thermograms of the semi-infinite model, we observe that the thermograms Tmod and Tsemiinfini coincide until 200 s (Figure 10a). This suggests that determining the slope α of the T vs. $t1/2$ thermogram (Figure 10.b) provides a reliable estimate of the thermal effusivity E between 100 and 125 s. By examining the linear section of the T vs. t thermogram (Figure 10.c), it is possible to make a reliable

preliminary assessment of the volumetric heat capacity ϱCpρCp between 300 and 500 s. Additionally, it is noted that this model does not minimise the sum of squared differences between the values of Texp and Tsemiinfini. This may be attributed to elevated contact resistances at the interface between the material and the heating resistor.
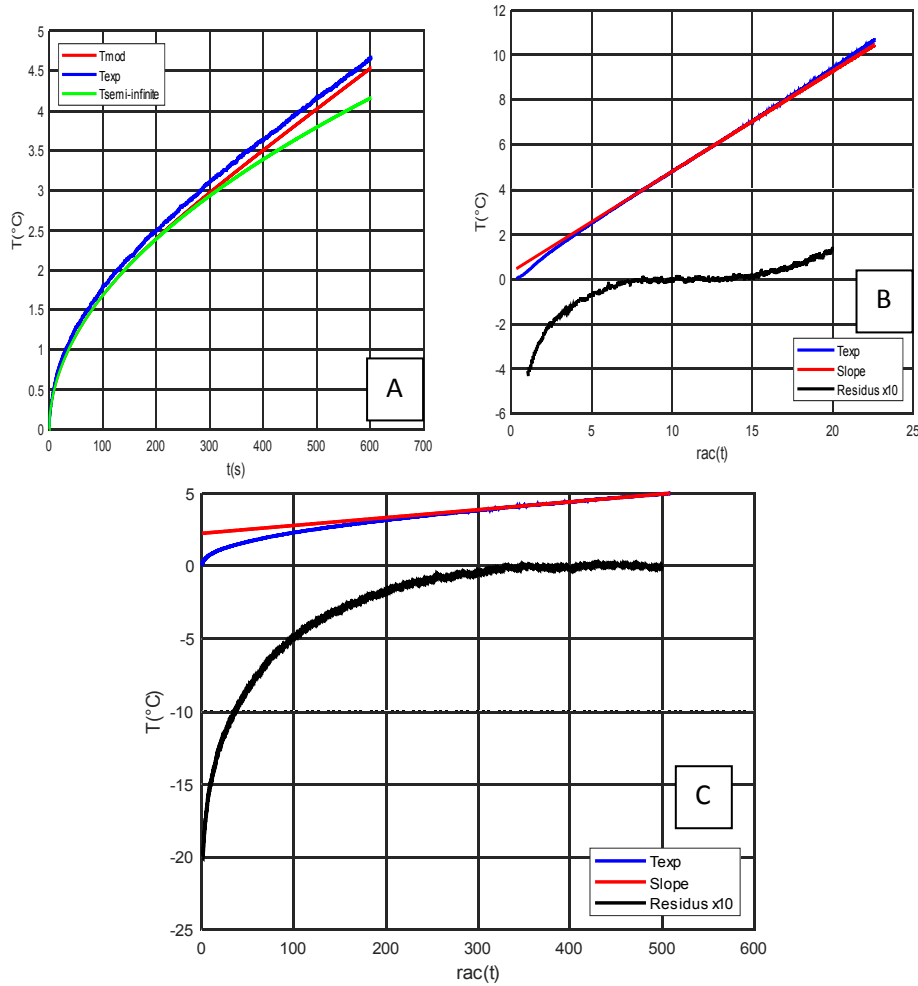
Figure 10: (A) Correlation between the semi-infinite thermograms Tsemi infini (equation 14) and Tsemi infini (equation 13) with the experimental results Texp for control sample C. Thermogram for pre-estimation: (B) slope α for thermal effusivity E estimation; (C) slope β for volumetric heat capacity ρCp estimation

The accurate value of thermal conductivity can only be confirmed if there is concurrence between the experimental findings (thermogram Texp=f(t1/2) and Texp=f(t)) and the formulated model (eq. 23). The permissible relative discrepancy is 8%. To do numerical modeling of the device (eq. 23), it is necessary to use the pre-estimated parameters from the simple model as input initially. These values are Epreest (eq. 15) and (ρCp) preest (eq. 16). By employing a convergence criterion, the accurate value of λ will thereafter be ascertained and juxtaposed with the pre-estimated value.

$$S_r(K,t) = K \cdot \frac{\partial T(K,t)}{\partial K}$$

To fully validate the measurement data, it is necessary to analyze the lowered sensitivities of the thermophysical parameters to temperature. Figures 11.a and 11.b display the thermograms with lower sensitivity for materials (control sample C1 and C2). Examination of these diminished sensitivity curves reveals that there is no association between the parameters E and ρCp (as depicted in figure 11.a). This demonstrates that the created model is indeed responsive to thermal effusivity and volumetric heat capacity, rendering it well-suited for precise estimation of thermal conductivity. The results are similar to those published by other authors [37-38].
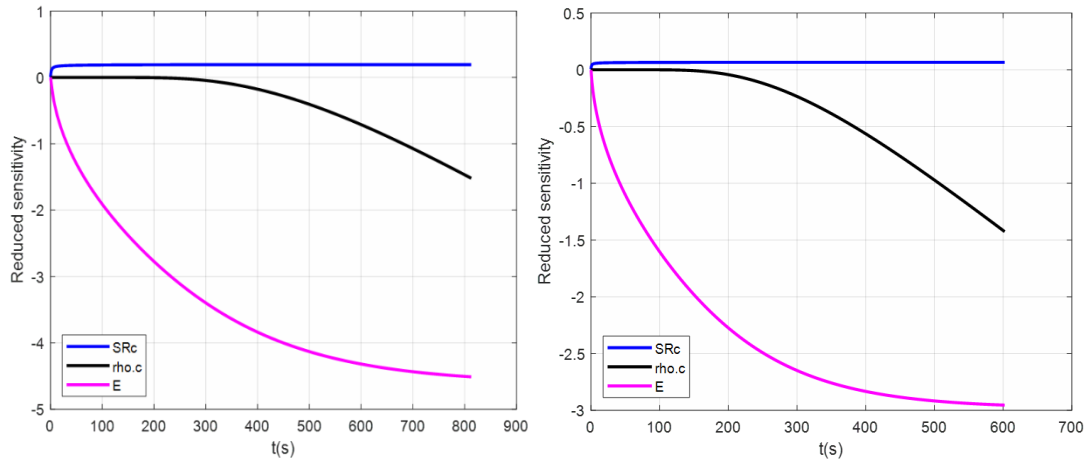
| A | | B |

Figure 11: Reduced sensitivity curve: (A) material C1; (B) material C2

Despite the first satisfaction with the simplified model and decreased sensitivity curves for the values of E and ρCp, Figure 10a examination reveals that the results cannot be validated due to the lack of convergence between the model curves (eq. 13, Tmod) and the experimental data (Texp). Hence, it is vital to conduct a study utilizing the Complete model.

Estimation from the Complete Model
A numerical simulation was conducted using the complete model, utilizing the beginning values of E and ρCp obtained from the simplified model (equations 15 and 16). The results of the simulation indicate that there is convergence between the temperatures predicted by the model and those observed in the experiments. This is illustrated in Figure 12.a, which displays the results for sample C1 and additional samples. This further confirms the precision of the established model in calculating the thermophysical parameters of these materials.
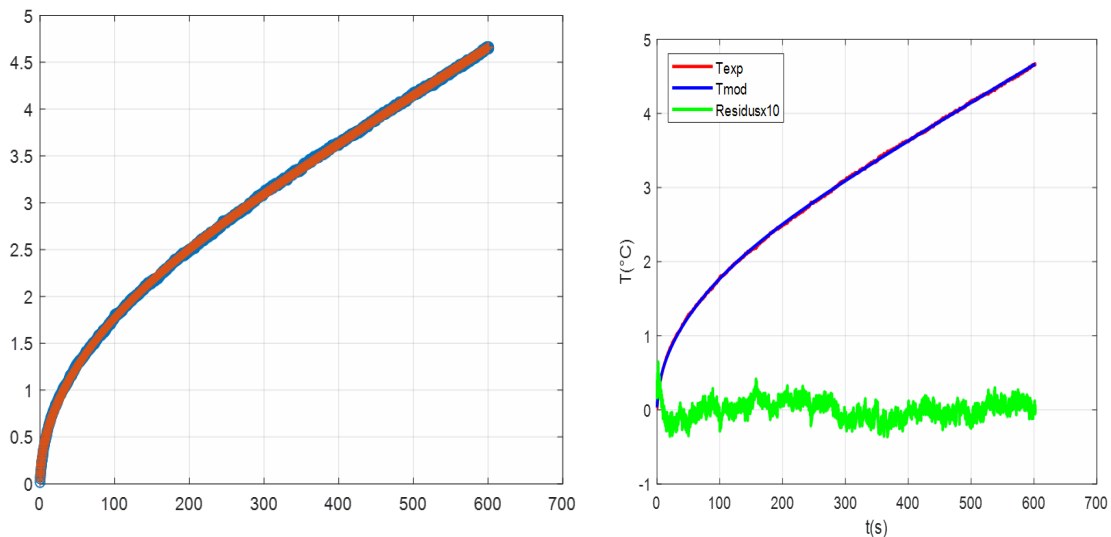

Figure 12:(A) initial probe inertia (B) displays of the thermograms obtained from the comprehensive model for sample C1.

Figure 12b displays the thermograms T=f(t) obtained from the comprehensive model for sample C1. The presence of initial probe inertia is seen (Figure 12.a). The absence of complete convergence of the estimation residues (green curves) towards the center zero may be attributed to elevated water content, irregular material surfaces, elevated contact resistances, and surface roughness, as observed in the case of sample C1.

Thermal properties of coconut and spikelet fibres reinforced bricks
Thermal Conductivity
Summary of thermal performance parameters is provided in table 2

Table 2: Average thermal conductivity of coconut and spikelet fiber samples

% OF COCONUT AND SPIKELET FIBRES	% NAOH	0	0.5	1	1.5	2	2.5
AVERAGE THERMAL CONDUCTIVITIES(W/MK)	A1	0.863	0.774	0.663	0.570	0.490	0.423
	A2	0.863	0.803	0.773	0.707	0.638	0.576
	A3	0.863	0.763	0.689	0.622	0.562	0.507
	A4	0.863	0.814	0.751	0.692	0.638	0.589
	B1	0.863	0.733	0.623	0.53	0.45	0.383
	B2	0.863	0.78	0.763	0.687	0.618	0.556
	B3	0.863	0.743	0.669	0.602	0.542	0.487
	B4	0.863	0.794	0.731	0.672	0.618	0.569
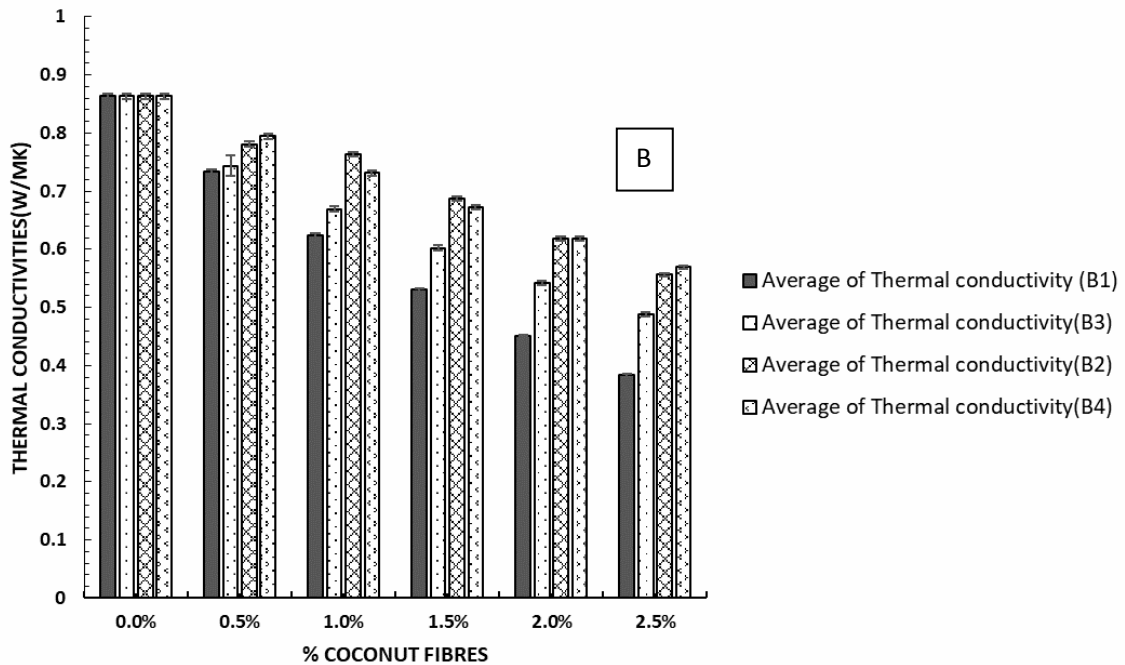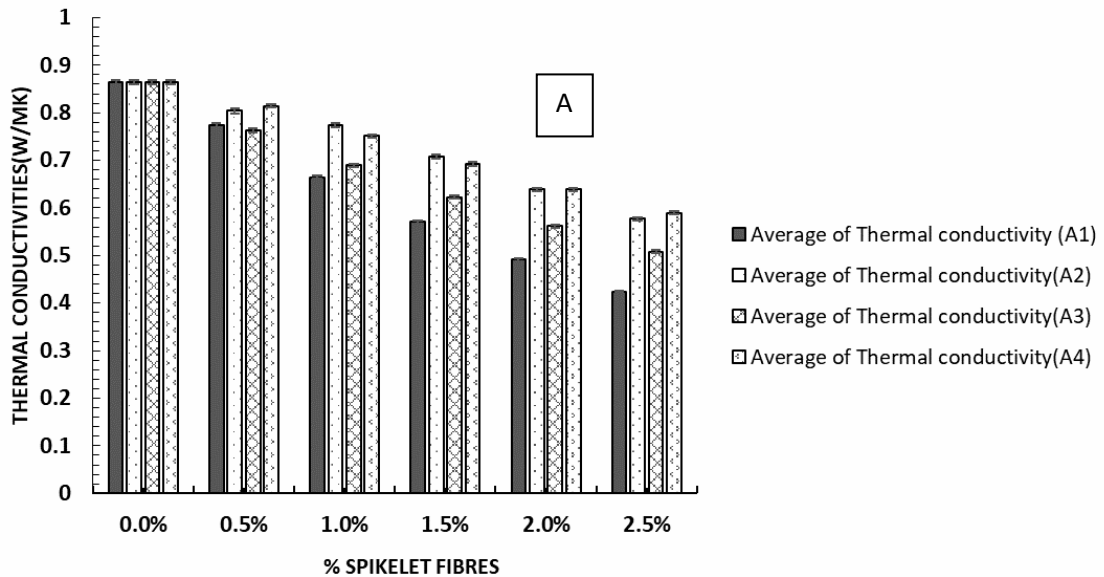
Figure 13: Thermal conductivity of bricks as function of (A) spikelet fibres (%) and (B) coconut fibres (%)

The ability of a material to conduct heat is an important factor in figuring out how energy-efficient it is. The change in heat conductivity as a function of EFBSF and CF is shown in Figures 13a and 13b above. The results show that as the amount of plant material increases, the visible thermal conductivity of the composite

material goes down. The heat-conducting properties of coconut and spikelet fibers that were treated with NAOH at 1 to 4% (B1, B2, B3, B4 for CF) and (A1, A2, A3, A4 for EFBSF) with different amounts of organic waste (0.5 to 2.5%, respectively). When the CF and EFBSF levels are raised by 0 to 2.5% compared to the reference, the thermal conductivity drops by 55.61% (B1), 35.53(B2), 43.56% (B3), and 34.07% (B4). For CF and 50.99%(A1), 33.21%(A2),41.19% (A3) and 31.77%(A4). With the lowest thermal conductivity of 0.383 W/Mk for CF and 0.423 W/Mk for SF This drop in thermal conductivity could be because of the high mass density. Also, spikelet and coconut fibers are lighter than ground volume, so the steady replacement of ground volume with vegetable matter makes it less thermally conductive. [39-41,8,47]
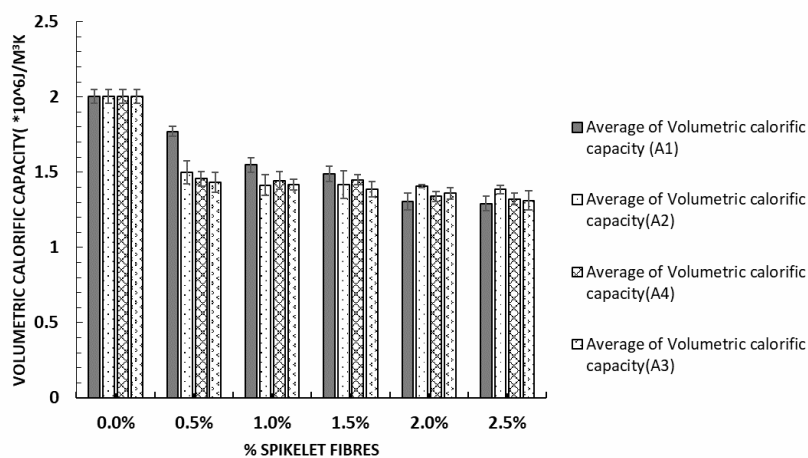
volume calorific capacity

The average volumetric calorific capacity of coconut fibers (CF) and empty fruit bunch spikelet fibres (EFBSF) is shown in Table 3.

Table 3: The average volumetric calorific capacity of coconut fibers (CF) and empty fruit bunch spikelet fibres (EFBSF)

% OF COCONUT AND SPIKELET FIBRES	% NAOH	0	0.5	1	1.5	2	2.5
AVERAGE VOLUMETRIC CALORIFIC CAPACITY(*10^6J/M3K)	A1	2	1.77	1.54	1.48	1.3	1.29
	A2	2	1.49	1.41	1.41	1.4	1.38
	A3	2	1.43	1.41	1.38	1.35	1.3
	A4	2	1.45	1.44	1.44	1.33	1.32
	B1	2	1.71	1.75	1.7	1.66	1.63
	B2	2	1.6	1.5	1.46	1.37	1.26
	B3	2	1.75	1.61	1.6	1.48	1.41
	B4	2	1.93	1.84	1.76	1.67	1.64
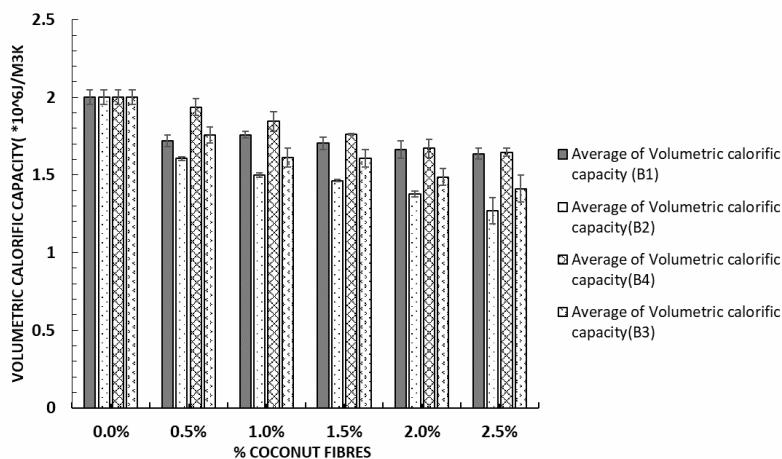
Figure 14: volumetric calorific capacity of samples (A) coconut fibres(B) spikelet fibres
 The hot plate device was used to measure the volume calorific capacity. Comparative analysis of thermal volumetric calorific capacity indicates that both spikelet and coconut fibres, when treated with NaOH and incorporated into earth bricks, effectively reduce the heat storage capacity of the bricks. Bricks have varying values in terms of CF and EFBSF, as seen in Figures 14a and 14b above. As the percentage of CF and EFBSF in the brick increases, the results demonstrate a linear decrease in volume calorific capacity with a variation of 18.23% (B1) 36.55%(B2), 29.42%(B3), 17.76%(B4) in the volumetric heat capacity between pure brick and brick containing 2.5% of agricultural residues, as well as 35.46%(A1), 30.84%(A2), 34.42%(A3), and 33.96%(A4) in the amount of energy required to raise the temperature of a unit volume (usually one cubic meter or one cubic centimeter of a substance by one degree Celsius or kelvin). They would be appropriate for use in hot climates due to their increased specific heat capacity, which is a result of the higher fiber content. Consistent with previous research, our findings demonstrate that insulating materials absorb heat at higher rates than non-insulating ones [8,42,39].

Thermal Effusivity
 Table 4 displays the average thermal effusivity of samples with varying fiber content ant treatment concentrations. This table provides a detailed summary of how different fiber contents and treatment levels affect the thermal effusivity of the samples.

Table 4: thermal effusivity of samples with varying fibre content and treatment concentration

% OF COCONUT AND SPIKELET FIBRES	% NAOH	0	0.5	1	1.5	2	2.5
	A1	1771.43	1519.97	1445.29	1309.61	1221.97	1219.6
	A2	1771.43	1358.55	1319.26	1240.78	1232.08	1168.52
	A3	1771.43	1300.62	1283.29	1276.298	1167.12	1183.5
Average thermal Effusivity (j/m2ks1/2)	A4	1771.43	1488.19	1379.92	1342.83	1264.81	1242.94
	B1	1771.43	1763.87	1620.62	1492.41	1487.37	1448.13
	B2	1771.43	1447.81	1394.81	1320.65	1207.69	1205.35
	B3	1771.43	1394.59	1355.81	1373.4	1328.84	1079.39
	B4	1771.43	1675.36	1444.74	1557.02	1552.1	1450.92
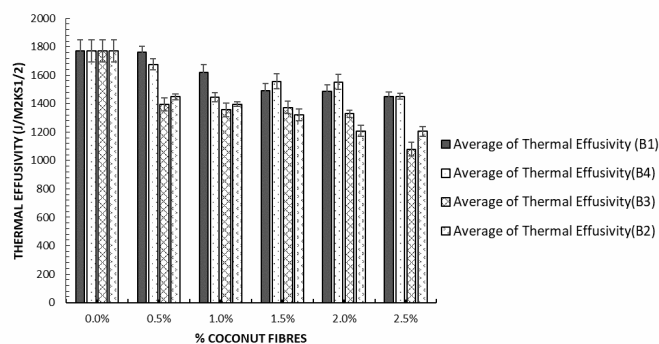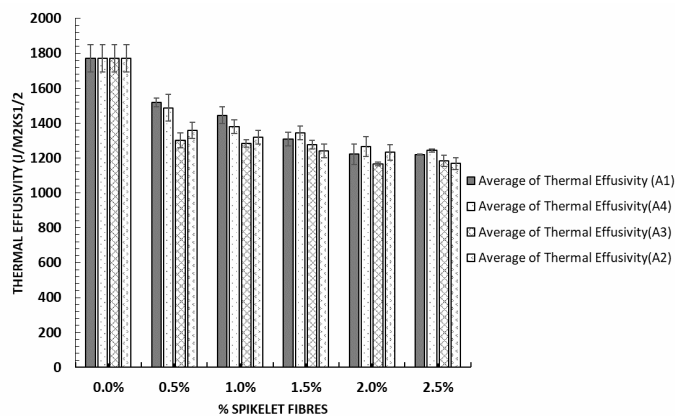
Figure 15: thermal effusivity of samples(A) spikelet fibres, (B)coconut fibres

Figures 15a and 15b above demonstrate that the thermal diffusivity has a similar trend to the thermal conductivity, decreasing as the proportion of addition increases. In order to effectively delay the transfer of heat flow, an insulating material must possess both a low thermal conductivity and a high level of insulation. The thermal diffusivity is observed to diminish when CF and EFBSF are added. The thermal effusivity of the reference brick B1, which is 1771.43 J/m²Ks^1/2, decreased by 18.25% compared to the brick with 2.5% CF, which has a thermal effusivity of 1448.13 J/m²Ks^1/2, B2 has a permeability of 1205.35 J/m²Ks^1/2, decreased by 31.95% with 2.5% CF. Similarly, B3 has a permeability of 1079.39 J/m²Ks^1/2, decreased by 39.06% with 2.5% cf. B4 also has a permeability of 1450.92 J/m²Ks^1/2, decreased by 18.09% with 2.5% CF. For spikelet fibres, A1 has a permeability of 1219.60 J/m²Ks^1/2, decreased by 31.15% with 2.5% SF. Similarly, A2 has a permeability of 1168.52 J/m²Ks^1/2, decreased by 34.03% with 2.5% SF. A3 also has a permeability of 1183.5 J/m²Ks^1/2, decreased by 33.18% with 2.5% SF. Finally, A4 has a permeability of 1242.94 J/m²Ks^1/2, decreased by 29.83% with 2.5% SF. The thermal performance of a composite is influenced by elements such as the percentage of fiber added, the mix of components, and the availability of pores for effusion. In order to be considered an insulating material, it is necessary for it to possess both a low thermal conductivity and a high capacity to impede the transfer of heat. [8],44-47].

IV. Conclusion

This study thoroughly investigated the thermal characteristics of termite mold soil, incorporating coconut and spikelet fibers. The composition of the fibers ranged from 0% to 2.5%, and they were treated with concentrations of sodium hydroxide varying from 1% to 4%. Our analysis revealed important findings about the impact of fiber type and NaOH treatment percentages on the thermal efficiency of these innovative composite materials. Coconut fibers consistently shown higher thermal performance compared to spikelet fibers in all investigated aspects. Their thermal effusivity and volumetric calorific capacity were increased, while their thermal conductivity remained lower. This confirms that they are effective reinforcements for improving thermal efficiency in termite mold bricks.

1) The most effective treatment for Spikelet Fibers was determined to be a 1% NaOH treatment, consistently resulting in superior thermal characteristics in terms of effusivity, volumetric calorific capacity, and thermal conductivity. This treatment achieves a suitable equilibrium between improving thermal properties and ensuring practical usefulness. The thermal characteristics of spikelet fibers showed a steady improvement as the composition increased, reaching its peak at 2%. This indicates that a fiber content of approximately 2%, along with a 1% NaOH treatment, can optimize the thermal efficiency of termite mold bricks with a thermal effusivity (E): 1221.98 J/m2Ks1/2, Density-specific heat capacity (ρCp) 1.304 *10^6J/M³K, showing efficient heat capacity and thermal conductivity (λ) 0.490 W/mK the lowest among all spikelet samples, reflecting excellent insulation.at 2.5% content and 1%NaOH spikelet fibres also perform well, but the thermal conductivity 0.423 W/mK (although low) is accompanied by higher effusivity of 1219.608 J/m2Ks1/2 and specific heat capacity of 1.291*10^6J/M³K making 2% fibre content a more balanced choice

2) Coconut fibers exhibited the best thermal properties when subjected to a 1% NaOH solution, consistently displaying greater thermal effusivity, volumetric calorific capacity, and reduced thermal conductivity. These characteristics emphasize their efficacy in improving thermal efficiency. Coconut fibers exhibited consistent thermal properties up to a concentration of 2.5% in relation to their fiber content. At this particular level of composition and after being treated with a 1% NaOH solution, they demonstrated the highest level of thermal efficiency, making them well-suited for applications that demand efficient heat management with a thermal effusivity (E): 1448.138J/m2Ks1/2, Density-specific heat capacity (ρCp) 1.636 *10^6J/M³K, showing efficient heat capacity and thermal conductivity (λ) 0.383 W/Mk the study determines that spikelet fibers treated with 1% NaOH at a composition of 2% and coconut fibers treated with 1% NaOH at a composition of 2 .5% are the most efficient designs for improving the thermal properties of termite mold bricks. These findings provide useful insights for designing sustainable building materials that enhance thermal efficiency and contribute to environmental conservation efforts. Future research could focus on enhancing the mechanical and environmental properties of these composites, thereby broadening their practical uses and driving progress in construction technology. By further improving these characteristics, we can fully exploit the capabilities of eco-friendly construction materials, fostering advancements that are advantageous to both the industry and the environment.

V. Acknowledgments

Conflict Of Interest

The authors have no conflicts of interest related to the publication of this paper.

Funding

References

[1] Jannot, Y., Remy, B., & Degiovanni, A. Measurement Of Thermal Conductivity And Thermal Resistance With A Tiny Hot Plate2009 High Temperatures-High Pressures 39 11-31

[2] Mohameth Dia, Mactar Faye, Mamadou Salif Diallo And Vincent Sambou, Measurement Of The Thermal Properties Of Materials By The Hot Plate Method Considering The Convection Coefficient Around The Device Mater. Res. Express 10 (2023) 065502 DOI: 10.1088/2053-1591/Acdce

[3] Eric, K. , Damfeu, J. , Ursulala, P. , Ducourneau, J. , Woafo, P. And Pettang, C. (2021) Thermophysical And Mechanical Characterization Of Poto-Poto Compressed Blocks For Use As Fill Material. Materials Sciences And Applications, 12, 437-459. Doi: 10.4236/Msa.2021.1210029.

[4] Ouedraogo, M., Bamogo, H., Sanou, I., Mazars, V., Aubert, J.E. And Millogo, Y. (2023) Microstructural, Physical And Mechanical Characteristics Of Adobes Reinforced With Sugarcane Bagasse. Buildings, 13, Article 117. Https://Doi.Org/10.3390/Buildings13010117

[5] Ouedraogo, M., Et Al. (2019) Physical, Thermal And Mechanical Properties Of Adobes Stabilized With Fonio (Digitaria Exilis) Straw. Journal Of Building Engineering, 23, 250-258. Https://Doi.Org/10.1016/J.Jobe.2019.02.005

[6] Zhang, L., Yang, L., Jelle, B.P., Wang, Y. And Gustavsen, A. (2018) Hygrothermal Properties Of Compressed Earthen Bricks. Construction And Building Materials, 162, 576-583. Https://Doi.Org/10.1016/J.Conbuildmat.2017.11.163

[7] Dime, T., Sore, S.O., Nshimiyimana, P., Messan, A. And Courard, L. (2022) Comparative Study Of The Reactivity Of Clay Earth Materials For The Production Of Compressed Earth Blocks In Ambient Conditions: Effect On Their Physico-Mechanical Performances. Journal Of Minerals And Materials Characterization And Engineering, 10, 43-56. Https://Doi.Org/10.4236/Jmmce.2022.101004

[8] Modjonda, Souaibou, Etienne, Y. And Raidandi, D. (2023) Thermal And Mechanical Characterization Of Compressed Clay Bricks Reinforced By Rice Husks For Optimizing Building In Sahelian Zone. Advances In Materials Physics And Chemistry, 13, 177-196. Doi: 10.4236/Ampc.2023.1310013.

[9] Kurmus, H. And Mohajerani, A. (2020) Recycling Of Cigarette Butts In Fired Clay Bricks: A New Laboratory Investigation. Materials, 13, Article 790. Https://Doi.Org/10.3390/Ma13030790

[10] Bessa, A., Bigas, J. And Gallias, J. (2004) Evaluation Of The Binding Contribution Of Mineral Additions To The Porosity, Compressive Strength And Durability Mortars.

[11] Moriarty, J.P. And Svare, T.I. (1976) Housing Materials And Methods For Tropical Africa. Batiment International, Building Research And Practice, 4, 28.

[12] ASTM D570 – 98(2010) E1. Standard Test Method For Water Absorption Of Plastics. ASTM D1037 – 12. Standard Test Methods For Evaluating Properties Of Wood-Base Fiber And Particle Panel Materials.

[13] Mijinyawa Y., Lucas E. B., And Adegunloye F. O., (2007). Termite Mound Clay As Material For Grain Silo Construction. Agricultural Engineering International: CIGR Journal.

[14] Yakum Reneta Nafu, Josepha Foba-Tendoebenezer Njeugna (2018)" Influence Of Empty Fruit Bunch Fiber On The Mechanical Properties Of Cement Stablised Soil" Asian Journal Of Engineering And Technology (ISSN: 2321 – 2462)

[15] Bertelsen, I.M.G., Belmonte, L.J., Fischer, G. And Ottosen, L.M. (2021) Influence Of Synthetic Waste Fibres On Drying Shrinkage Cracking And Mechanical Properties Of Adobe Materials. Construction And Building Materials, 286, Article ID: 122738. Https://Doi.Org/10.1016/J.Conbuildmat.2021.122738

[16] Jannot Y And Acem Z 2007 A Quadrupolar Complete Model Of The Hot Disc Meas. Sci. Technol. 18 1229–34

[17] Jannot, Y., Remy, B., & Degiovanni, A. Measurement Of Thermal Conductivity And Thermal Resistance With A Tiny Hot Plate2009 High Temperatures-High Pressures 39 11-31.

[18] Nitcheu, M. , Meukam, P. , Damfeu, J. And Njomo, D. (2018) Thermomechanical Characterisation Of Compressed Clay Bricks Reinforced By Thatch Fibres For The Optimal Use In Building. Materials Sciences And Applications, 9, 913-935. Doi: 10.4236/Msa.2019.912066.

[19] Karawacki E, Suleiman B M, Ul-Haq I And Nhi B 1992 An Extension To The Dynamic Plane Source Technique For Measuring Thermal Conductivity, Thermal Diffusivity, And Specific Heat Of Dielectric Solids Rev. Sci. Instrum. 63 4390–7

[20] S. V. Obame, A. D. O. Betené, P. M. Naoh, F. E. Betené, And A. Atangana, "Characterization Of The Neuropeltis Acuminatas Liana Fiber Treated As Composite Reinforcement," Results In Materials, Vol. 16, Article 100327, 2022.

[21] S. B. T. Youbi, N. R. S. Tagne, O. Harzallah Et Al., "Effect Of Alkali And Silane Treatments On The Surface Energy And Mechanical Performances Of Raphia Vinifera Fibres," Industrial Crops And Products, Vol. 190, Article 115854, 2022.

[22] Meukam, P., Jannot, Y., Noumowe, A. And Kofane, T.C. (2004) Thermo Physical Characteristics Of Economical Building Materials. Construction And Building Materials,18,437-443. Https://Doi.Org/10.1016/J.Conbuildmat.2004.03.010

[23] Damfeu, J.C., Meukam, P. And Jannot, Y. (2016) Modeling And Measuring Of The Thermal Properties Of Insulating Vegetable Fibers By The Asymmetrical Hot Plate Method And The Radial Flux Method: Kapok, Coconut, Groundnut Shell Fiber And Rattan.Thermochimicaacta,630,64-77. Https://Doi.Org/10.1016/J.Tca.2016.02.007

[24] Antar, M.A. (2010) Thermal Radiation Role In Conjugate Heat Transfer Across A Multiple-Cavity Building Block. Energy, 35, 3508-3516.Https://Doi.Org/10.1016/J.Energy.2010.04.055

[25] Capelas De Oliveira, E. (2019) Integral Transforms. Studies In Systems, Decision Andcontrol,240,115-167. Https://Doi.Org/10.1007/978-3-030-20524-9_4

[26] Abessolo Dieudonne,Biwole Achille Bernard,Fokwa Didier,G.K.Bernard And Y.B. Baah (2022) Physical,Mechanical And Hygroscopic Behaviour Oof Compressed Earth Blocks Stabilized With Cement And Reinforced With Bamboo Fibres. International Journal Of Engineering Research In Africa

[27] Petkova, R. And Zlatev, P. (2017) Thermal Insulating Properties Of Straw Filled Environmentally Friendly Building Materials. Vol. 13, 52-57.

[28] Nitcheu, M. , Meukam, P. , Damfeu, J. And Njomo, D. (2018) Thermomechanical Characterisation Of Compressed Clay Bricks Reinforced By Thatch Fibres For The Optimal Use In Building. Materials Sciences And Applications, 9, 913-935. Doi: 10.4236/Msa.2019.912066.

[29] Saad Raefat Mohammed Garoum, Najma Laaroussi, El Mehdi El Khattabi, Mohammed Rhachi (2018) An Extended Hot Plate Method For Measurement Of Thermal Conductivity Variation With Temperature Of Building Materials. 3rd International Conference On Energy Materials And Applications IOP Conf. Series: Materials Science And Engineering 446 (2018) 012007 IOP Publishing Doi:10.1088/1757-899X/446/1/01200

[30] Judith Korb. Thermoregulation And Ventilation Of Termite Mounds. Naturwissenschaften (2003) 90:212–219 DOI 10.1007/S00114-002-0401-4

[31] N. Al-Azad, M.F.M. Asril, M.K.M. Shah.A Review On Development Of Natural Fibre Composites For Construction Applications J. Chem. Eng. Mater. Sci., 9 (7) (2021), Pp. 1-9, 10.4236/Msce.2021.97001

[32] Kosheela Devi Poopalam, Tuan Noor Maznee Tuan Ismail, Nurul 'Ain Hanzah, Aisyah Humaira Alias, Noorshamsiana Abdul Wahab, Zawawi Ibrahim, Vijaya Subramaniam, Abu Hassan Noor Armylisas, Zainab Idris, Utilization Of Oil Palm Biomass And Polyurethanes As Sustainable Construction Materials: A Review, Developments In The Built Environment, Volume 17, 2024, 100380, ISSN 2666-1659, Https://Doi.Org/10.1016/J.Dibe.2024.100380.

[33] Bonoli, A.; Zanni, S.; Serrano-Bernardo, F. Sustainability In Building And Construction Within The Framework Of Circular Cities And European New Green Deal. The Contribution Of Concrete Recycling. Sustainability 2021, 13, 2139. Https://Doi.Org/10.3390/Su13042139

[34] Mor Diarra Ndiaye, M., Touré, P.M., Dieye, Y. And Gueye, P.M. (2019) Thermo-Mechanical Characterization Of Building Component With Crushed Millet Stalk Fiber. International Journal Of Innovation And Applied Studies, 26, 1230-1239.

[35] Jannot, Y. (2011) Metrologie Thermique. Lab. d'Energétique Mécanique Théorique Appliquée, 6-97.

[36] Tonye Emmanuel, M. And Duval Roger, P.M. (2004) Caracterisation De Materiaux Locaux En

[37] Mor Diarra Ndiaye, M., Touré, P.M., Dieye, Y. And Gueye, P.M. (2019) Thermo-Mechanical Characterization Of Building Component With Crushed Millet Stalk Fiber. International Journal Of Innovation And Applied Studies, 26, 1230-1239.

[38] Dieye, Y., Sambou, V., Faye, M., Thiam, A., Adj, M. And Azilinon, D. (2017) Thermo-Mechanical Characterization Of A Building Material Based On Typha Australis. Journal Of Building Engineering, 9, 142-146. Https://Doi.Org/10.1016/J.Jobe.2016.12.007

[39] Babé, C., Et Al. (2020) Thermomechanical Characterization And Durability Of Adobes Reinforced With Millet Waste Fibers (Sorghum Bicolor). Case Studies In Construction Materials, 13, E00422. Https://Doi.Org/10.1016/J.Cscm.2020.E00422

[40] El-Sayed Ali, M. And Zeitoun, O.M. (2012) Discovering And Manufacturing A New

[41] Natural Insulating Material Extracted From A Plant Growing Up In Saudi Arabia. Journal Of Engineered Fibers And Fabrics, 7, 88-94.
Https://Doi.Org/10.1177/155892501200700405

[42] Millogo, Y., Morel, J.C., Aubert, J.E. And Ghavami, K. (2014) Experimental Analysis Of Pressed Adobe Blocks Reinforced With Hibiscus Cannabinus Fibers. Construction And Building Materials, 52, 71-78.
Https://Doi.Org/10.1016/J.Conbuildmat.2013.10.094

[43] Emir, I. (2008) Effect Of Organic Residues Addition On The Technological Properties Of Clay Bricks. Waste Management, 28, 622-627.
Https://Doi.Org/10.1016/J.Wasman.2007.03.019

[44] Benazzouk, A., Douzane, O., Mezreb, K., Laidoudi, B. And Quéneudec, M. (2008) Thermal Conductivity Of Cement Composites Containing Rubber Waste Particles: Experimental Study And Modelling. Construction And Building Materials, 22, 573-579. Https://Doi.Org/10.1016/J.Conbuildmat.2006.11.011

[45] Lahouioui, M. (2019) Elaboration Et Évaluation Des Propriétés Physico-Thermiques Et Acoustiques De Nouveaux Éco-Composites À Base De Bois De Palmier.

[46] Moretti, E., Belloni, E. And Agosti, F. (2016) Innovative Mineral Fiber Insulation Panels For Buildings: Thermal And Acoustic Characterization. Applied Energy, 169, 421-432. Https://Doi.Org/10.1016/J.Apenergy.2016.02.048

[47] Akpabio LE,Samuel DE, Sunday EE , Kufreabasi Thermal Properties Of Oil And Rafia Palm Fibres.Global Journal Of Pure And Applied Science 2001; 7(3); 575-578

[48] Yakum R. N., Noubissie T.R. L., Mbou .T. E, Foba J. T. (2022). Influence Of Palm Oil Mesocarp Fibres On The Thermal Properties Of Cement-Stabilized Compressed Earth–Based Brick. European Journal Of Engineering And Technology Research, 7(6), 9. Doi:Org/10.24018/Ejeng.2022.7.6.2910